

REPORT



Influence of physicochemical properties on the subcutaneous absorption and bioavailability of monoclonal antibodies

Amita Datta-Mannan^a, Selina Estwick^b, Chen Zhou, Hiuwan Choi^c, Nicole E. Douglass^d, Derrick R. Witcher^c, Jirong Lu^c, Catherine Beidler^c, and Rohn Millican^c

^aDepartments of Exploratory Medicine and Pharmacology, Lilly Research Laboratories, Lilly Corporate Center, Indianapolis, IN, USA; ^bExternal Innovation, Lilly Research Laboratories, Lilly Corporate Center, Indianapolis, IN, USA; ^cBiotechnology Discovery Research, Lilly Research Laboratories, Lilly Corporate Center, Indianapolis, IN, USA; ^dClinical Design/Delivery/Analytics, Lilly Research Laboratories Lilly Corporate Center, Indianapolis, IN, USA

ABSTRACT

Many therapeutic monoclonal antibodies (mAbs) were initially developed for intravenous (IV) administration. As a means to improve mAb drug-ability and the patient experience, subcutaneous (SC) administration is an increasingly important delivery route for mAbs. Unlike IV administration, bioavailability limitations for antibodies have been reported following SC injection and can dictate whether a mAb is administered via this parenteral route. The SC bioavailability of antibodies has been difficult to predict, and it can be variable and partial, with values ranging from ~50% to 100%. The mechanisms leading to the incomplete bioavailability of some mAbs relative to others are not well understood. There are some limited data that suggest the physicochemical properties inherent to a mAb can contribute to its SC absorption, bioavailability, and *in vivo* fate. In this study, we evaluated the integrated influence of multiple mAb physicochemical factors on the SC absorption and bioavailability of six humanized mAbs in both rats and cynomolgus monkeys. We demonstrate the physicochemical properties of mAbs are critical to their rate and extent of SC absorption. The combination of high positive charge and hydrophobic interaction significantly reduced the rate of the evaluated mAb's SC absorption and bioavailability. Reduction or balancing of both these attributes via re-engineering the mAbs restored desirable properties of the molecules assessed. This included reduced association with SC tissue, improvements in mAb absorption from the SC space and overall SC bioavailability. Our findings point to the importance of evaluating the relative balance between various physicochemical factors, including charge, hydrophobicity, and stability, to improve the SC drug-ability of mAbs for selecting or engineering mAbs with enhanced *in vivo* absorption and bioavailability following SC administration.

ARTICLE HISTORY

Received 30 October 2019
Revised 24 April 2020
Accepted 8 May 2020

KEYWORDS



Subcutaneous absorption; subcutaneous bioavailability; monoclonal antibody; physicochemical characterization; hydrophobicity; thermal stability; chemical properties; charge; nonspecific binding; drug-ability; pharmacokinetics; disposition

Introduction

Over the past few decades, human or humanized monoclonal antibody (mAb) pharmaceuticals have been successfully used as therapeutic modalities in a wide array of human diseases due to their target binding specificity, bivalent interaction properties, potential to have innate effector function and their *in vitro* and *in vivo* biochemical stability.^{1,2} Advances in antibody engineering methods, such as humanization, potency and specificity optimization, for achieving the ideal pharmacodynamics (PD) and improvements in the drug-ability properties, such as pharmacokinetics (PK), are vital to the success of mAb-based therapies. While some of these engineering approaches have enhanced the pharmacokinetic/pharmacodynamic (PK/PD) properties by reducing mAb dose and/or dose frequency, considerable opportunities remain in this space. More recently, one of the increased areas of intense attention for improving/engineering the PK properties of mAbs has involved understanding the fate and bioavailability of mAbs following subcutaneous (SC) administration.

Relative to the intravenous (IV) route, SC administration is generally preferred for therapeutic antibodies in clinical settings due to increased patient convenience and compliance,^{3,4} but bioavailability limitations associated with SC injection can reduce systemic exposure. The bioavailability of mAbs has been difficult to predict following SC administration, can be variable and partial with values of ~50% to 100%.^{5–7} Currently, the SC bioavailability for marketed mAbs in humans is ~60–80%.^{4,6,8} While the mechanisms related to the incomplete bioavailability observed for some mAbs are not well understood, there is a general consensus that the PK fate and absorption profile of mAbs following SC administration requires an understanding of the SC space/anatomy and composition.

The SC matrix or hypodermis has been reviewed extensively.^{4,6,8} Briefly, the hypodermis is composed of connective tissue separated by fat lobules (adipose tissues) and cellular components, including adipose cells, fibroblast and macrophages. The fibroblasts are responsible for producing constituents of the extracellular matrix (ECM), including glycosaminoglycans (GAGs), elastin and collagen. GAGs are

CONTACT Amita Datta-Mannan  datta_amita@lilly.com  Lilly Research Laboratories, Eli Lilly & Company, Lilly Corporate Center, Indianapolis, IN 46285, USA.

At the time the work in this publication was completed all authors were or are current employees of Eli Lilly and Company. The authors do not have any conflict of interest or financial disclosure to report.

© 2020 The Author(s). Published with license by Taylor & Francis Group, LLC.

This is an Open Access article distributed under the terms of the Creative Commons Attribution-NonCommercial License (<http://creativecommons.org/licenses/by-nc/4.0/>), which permits unrestricted non-commercial use, distribution, and reproduction in any medium, provided the original work is properly cited.

highly negatively charged polysaccharides; the most common GAG in the SC space is hyaluronic acid. The strong negatively charged GAGs control the interstitial fluid content and hydraulic conductivity or movement of endogenous and exogenous entities within the interstitium. The macrophage and dendritic cells within the hypodermis function as a host defense mechanism by facilitating catabolism and sequestration of foreign antigens/substrates before these entities proceed into the blood circulation. In terms of structure, the SC tissue milieu is somewhat vascularized with mostly small blood capillaries and lymphatic vessels, both of which can provide access to the general circulation.

Several studies have demonstrated that for larger molecular weight moieties (>16 kDa), such as mAbs (~150 kDa), the SC capillaries are practically impermeable with regard to passive permeability; thus, as a class of molecules, lymphatic uptake from the interstitial space plays a key role in eventual absorption of mAbs into systemic circulation.⁹⁻¹¹ Of note, another potential mechanism that may affect mAb SC absorption is active transport by the neonatal Fc receptor (FcRn) across the capillary endothelia. Some studies have reported the involvement of FcRn in the SC absorption of mAbs, suggesting it is an important, yet potentially saturable, uptake mechanism for mAbs.¹²⁻¹⁴ There are, however, conflicting reports with mixed results on how FcRn can be leveraged to affect mAb SC absorption and bioavailability, implying there may be additional mAb-centric considerations with regard to leveraging FcRn as a platform-based modality for improving mAb SC absorption.¹²⁻¹⁴ Regardless of the balance of blood or lymph capillary uptake of mAbs, after SC administration the mAb must be shunted through the interstitium to reach these capillaries. Given the mixture of cells (adipocytes, macrophages and fibroblasts) and matrices (adipose, GAGs, proteoglycans, elastin and collagen), it is reasonable to speculate that the PK fate, absorption profile and engineering strategies for improving mAb SC kinetics require an understanding of the interplay of the molecule's physiochemical properties with the SC space and anatomy discussed above.

Interestingly, while the number of mAb-based biological therapies have increased, there is still quite a bit of debate and a paucity of information around the relative balance between physiochemical characteristics and their effects on mAb PK. This has led to inadequate understanding of how these parameters might affect absorption processes for mAbs administered to the SC space. As previously noted, some limited physiochemical elements such as the molecular weight and FcRn binding capacity have been interrogated.⁹⁻¹⁴ In addition, some studies have been conducted with charge-based mAb variants with mixed findings. In a study by Khawli *et al.*, no significant differences in SC absorption were reported with IgG1 charge variants; however, the pI of these IgG1 molecules varied marginally (within 0.1 isoelectric point (pI) units), and thereby may not have been different enough to affect SC absorption.¹⁵ In contrast, in another report, mAbs with a broader range of pI (1 unit differences) showed a moderate trend correlating increasing mAb pI and decreasing SC bioavailability.¹⁶ Consistent with the later findings, Mach and coworkers reported that positively charged mAbs interact *in vitro* with SC tissue, likely mediated via electrostatic

interactions.¹⁷ Taken together, these studies have started to illuminate the role of intrinsic mAb physiochemical features on the rate and extent of SC absorption, but there is a scarcity of data for factors such as the hydrophobicity, thermal stability, and aggregation potential of mAbs following SC injection, as well as the interplay of these factors with charge, pI and FcRn binding interactions. Defining the relative contribution of the multiple factors affecting mAb SC disposition is critical to guiding rational molecule design, engineering, selection and improving drug-ability for better therapeutic outcomes/experiences for patients. Given these considerations, herein, broader evaluations of the impact that various mAb physiochemical parameters may have with the SC tissue environment, absorption processes and PK of mAbs in an integrated manner were conducted.

The goal of our investigation was to collate these concepts by characterizing the effects of charge, hydrophobicity, aggregation potential and thermal stability on the rate and extent of SC absorption of six humanized mAbs separated into three families in rats and/or cynomolgus monkeys. The three mAb families were characterized by differences in charge- or hydrophobic-based interactions with *in vitro* matrices. MAbs with increased charge-based or increased hydrophobic interaction potential showed reduced exposure characterized by slower rates of absorption and a decreased extent of SC absorption in rats compared to molecules that did not have positive charge patches in the complementarity-determining region (CDR). These findings were further confirmed in cynomolgus monkeys, as poorly absorbed molecules with increased charge-based or increased hydrophobic interaction potential had larger amounts of mAb remaining at the SC injection site compared to mAbs without these factors. Moreover, while the absolute exposure findings in cynomolgus monkeys were different than rats for a subset of the evaluated mAbs, the relative rank order of SC bioavailability were directionally similar across the two species. In addition, greater connectivity between the SC PK of the evaluated mAbs and the onset temperature for tertiary structure unfolding propensity, as well as the temperature at which aggregation was induced, was observed than for the IV PK of the same mAbs. Taken together, the data suggest certain physiochemical parameters may be more connected and unique to the PK performance of mAbs following SC administration than IV dosing. These results point to the importance of integrating and understanding both the physiochemical characteristics of the mAb and the interplay with the mechanisms/physiological components of the SC space in guiding the application of optimal engineering and screening strategies to deliver mAb-based therapies via the SC route.

Results

Description of the IgG molecules

In this study, we leveraged six humanized IgG molecules, across three platforms, to characterize the connectivity between mAb physiochemical properties and PK parameters following SC administration. Table 1 lists the constructs and a high-level summary of their qualitative biophysical

Table 1. General description of the mAbs^a

Platform	mAb	mAb isotype	Charge-based interaction potential	Hydrophobic-based interaction potential	T _{agg} ^b	TMDD In rats ^c	TMDD in cynomolgus monkeys ^c
1	1P	IgG1	+++	-	-	-	-
	1RE	IgG1	++	-	-	-	-
2	2P	IgG4	+++++++	++	++	-	+
	2RE	IgG4	++++	++	+	-	+
3	3P	IgG4	++	+++	++	-	-
	3RE	IgG4	+	+	-	-	-

^aAll the molecules are humanized IgGs. The '+' and '-' signs indicate the presence and absence of a characteristic, respectively. The number of '+' symbols within the charge- and hydrophobic-based interaction potential columns are intended to provide a qualitative perspective of the relative preponderance of each characteristic across and within the mAb platforms. Quantitative values for the charge- and hydrophobic-based interaction potential are in Table 2. ^bT_{agg} is the temperature of aggregation onset. ^cTMDD = target-mediated drug disposition.

properties. Each antibody platform was developed against a different undisclosed target. Within each platform, two mAbs were characterized: a parent molecule and a re-engineered mAb that was designed to have physiochemical property changes distinct from the parent (proprietary sequence changes are not disclosed). Platform 1 is composed of two humanized IgG₁ molecules, including the parent (P) mAb 1P and the re-engineered (RE) mAb 1RE. Platforms 2 and 3 each consist of two humanized IgG₄ constructs. The molecules in Platform 2 are the parent mAb 2P and the re-engineered mAb 2RE. Platform 3 consists of the parent mAb 3P and the re-engineered mAb 3RE. Overall, the three platforms were leveraged to dissect the role of charge and hydrophobicity in mAb kinetics following SC administration. Platform 1 molecules were leveraged to understand the role of charge, Platform 2 molecules had components of both charge and hydrophobicity, and Platform 3 molecules were predominantly influenced by hydrophobicity differences.

Characterization of the physiochemical properties of the mAbs

Table 2 summarizes the physiochemical attributes of the mAbs in each platform via a battery of analyses aimed at understanding the physiochemical profiling connected with the PK and absorption following SC administration. Molecular interactions governed by hydrophobic and charge-based mechanisms were evaluated using multiple orthogonal approaches. In addition, molecules were also assessed for overall thermal stability, as well as their aggregation potential.

The global molecule hydrophobicity was determined using a hydrophobic interaction chromatography (HIC)-based method. The data were expressed as a relative hydrophobicity interaction percentage for each of the mAbs to allow for comparisons both within and across the three mAb platforms; larger

hydrophobicity interaction percent (HIP) values indicate an increased affinity for the HIC matrix. The Platform 1 molecules show similar and relatively low HIP values; the HIP for mAb 1P and mAb 1RE were 1.3% and 0.7%, respectively. In contrast, both the Platform 2 and 3 molecules showed ~10- to ~100-times higher HIP values than the Platform 1 mAbs (Table 2). The Platform 2 constructs showed similar HIP values for mAb 2P and mAb 2RE of ~16% and ~20%, respectively. Platform 3 mAbs had the widest diversity of HIP, with mAb 3P and 3RE displaying values of ~100% and ~12%, respectively.

The charge of the mAbs was evaluated using multiple orthogonal approaches. Global mAb surface charge was assessed via determination of the pI and zeta potential, whereas local surface charge was determined through heparin-binding interactions. The pI values were determined using capillary isoelectrophoresis. Our results indicated some subtle differences in the pI of molecules when compared within and across each platform (≤ 0.2 units) (Table 2). The Platform 1 mAbs 1P and 1RE had pI values of 8.8 and 9.1, respectively; Platform 2 mAbs 2P and 2RE molecules had pI values of 9.2 and 9.0, respectively; and Platform 3 mAbs 3P and 3RE constructs had pI values of 8.3, 8.5, respectively (Table 2). The zeta potential of the mAbs was determined using electrophoretic light scattering. The zeta potential of the molecules tended to be similar with the exception of the non-significantly lower and higher potentials observed for mAbs 1P and 2P, respectively (Table 2). The interaction of the six mAbs with heparin was evaluated using a heparin-coated matrix packed into a column. Heparin was selected since it is found in abundance on the SC capillaries.⁴ Previously, we reported the interaction of molecules with heparin using heparin-coated plates.^{18,19} This method was dependent on the detection of heparin-bound mAbs using an antibody-based detection. Differences in the cross-reactivity of the mAbs with the detection antibody created challenges in the quantitative comparison of the heparin-binding across molecules (data not shown). Thus, in the context of this study, we chose to

Table 2. Biophysical and FcRn binding properties of the mAbs^a

Platform	mAb	FcRn K _d (nM) at pH 6	HpnIP (%)	HIP (%)	Zeta potential (mV)	pI	T _{agg} (°C)	T _{m onset} (°C)	T _m (°C)		
									C _{H2}	C _{H3}	Fab
1	1P	105 ± 5	51.8	1.3	6.2 ± 1.4	8.8	64.2 ± 0.5	61.1	67	83	70
	1RE	98 ± 10	28.3	0.7	9.5 ± 0.2	9.1	64.5 ± 0.2	61.7	70	83	70
2	2P	93 ± 4	100	16.0	10.5 ± 1.4	9.2	52.4 ± 2.1	56.6	69	72	76
	2RE	121 ± 15	58.1	20.1	9.7 ± 1.9	9.5	59.6 ± 1.1	62.0	69	73	76
3	3P	101 ± 7	31.6	100	9.4 ± 0.8	8.3	55.6 ± 2.3	58.9	69	73	68
	3RE	113 ± 4	18.6	11.7	9.7 ± 0.6	8.5	63.9 ± 2.7	62.2	69	73	78

^aFcRn K_d represents cynomolgus monkey FcRn binding affinity at pH 6. Abbreviations: HpnIP, relative heparin-binding interaction potential; HIP, relative hydrophobic interaction potential; pI, isoelectric point; T_{agg}, temperature of aggregation onset; T_{m onset}, onset of tertiary structure unfolding.

evaluate all three mAb platforms using a heparin column and UV-VIS-based detection to allow for adequate comparisons of the heparin interaction across molecules. The data were expressed as a relative heparin interaction percentage (HpnIP) for each of the mAbs to allow for comparisons both within and across the three mAb platforms; larger heparin interaction percent (HpnIP) values indicate an increased affinity for the heparin matrix. The Platform 1 molecules show an ~1.9-fold difference in HpnIP values; the HpnIP for mAbs 1P and 1RE were ~52% and ~28%, respectively. The Platform 2 molecules showed ~1.7-fold differences, with mAb 2P and mAb 2RE displaying ~100% and ~58% HpnIP values, respectively. The Platform 3 mAbs HpnIP values of mAb 3P and mAb 3RE were ~32% and ~19%, respectively.

The T_m of the mAbs was determined using differential scanning calorimetry (DSC). Within the three platforms, a higher onset of melting temperature ($T_{m \text{ onset}}$) was observed for mAb 1RE relative to 1P, mAb 2RE relative to 2P and mAb 3RE relative to 3P (Table 2). Differences in T_m values were observed in the antigen-binding fragment (Fab) regions within Platform 3, the C_{H2} domains of the Platform 1 molecules and the C_{H3} of the Platform 2 mAbs (Table 2). In addition to DSC, simultaneous static light scattering (SLS) and fluorescence spectroscopy were used to monitor aggregation (T_{agg}) and the onset temperature ($T_{m \text{ onset}}$) of tertiary structure unfolding. The parabolic nature of protein unfolding free energy dependence on temperature determines that at high temperature protein will readily unfold. During thermal ramping from moderate temperature, protein will be partially unfolded at certain points, and consequently will drive further intermolecular interactions and finally aggregation. SLS is sensitive to trace amount of aggregates and well suited for measuring aggregation onset. The unfolding event in the meantime will trigger red shifting of the fluorescence spectrum due to the exposure of aromatic amino acid and, in our case, tryptophan. Therefore, simultaneous SLS and fluorescence spectroscopy is able to capture the aggregation propensity and conformational stability at the same time during thermal ramping. The results are reported in Table 2. The temperature of aggregation onset (T_{agg}) of the Platform 1 mAbs 1P and 1RE were 64.2°C and 64.5°C, respectively. The T_{agg} increased in the Platform 2 mAbs from 52.4°C for mAb 2P to 59.6°C for mAb 2RE. In the case of Platform 3, the T_{agg} increased from 55.6°C for mAb 3P to 63.9°C for mAb 3RE. In the

meantime, the unfolding onset ($T_{m \text{ onset}}$) of the Platform 2 mAbs improved from 57.6°C to 62.0°C for mAbs 2P and 2RE, respectively, as well as for the Platform 3 mAbs from 58.9°C to 62.2°C for mAbs 3P and 3RE, respectively, after re-engineering (Table 2).

The binding affinities of mAbs with immobilized cynomolgus monkey FcRn (cFcRn) were measured using previously reported surface plasmon resonance (SPR) approaches.²⁰ The binding affinity (K_d) of the mAbs for cFcRn at pH 6.0 ranged from ~93 to 121 nM across the three mAb platforms. No direct binding to cFcRn at pH 7.4 was detected for any of the mAbs (data not shown).

Evaluation of the pharmacokinetics of the mAbs in rats

We chose to evaluate the PK of our constructs following a single IV or SC administration to rats due to the ability to serially sample individual animals over the duration of the *in vivo* study. In addition, in rats none of the molecules has a target-mediated component to their clearance (i.e., target-mediated drug disposition (TMDD)) either due to low endogenous antigen concentrations or the lack of the cross-reactivity of the antibodies with rat antigen. As a consequence, the inherent influence of the physiochemical parameters of the mAbs on PK could be evaluated in the absence of the kinetic complexities associated with TMDD.

The PK parameters following a single 1 mg/kg IV or SC administration of the six mAbs are reported in Table 3. Overall, the apparent clearance (CL/F) (and intrinsic clearance in the case of the IV administration), rate of SC absorption (k_a) and SC bioavailability of the re-engineered mAbs in each platform (1RE, 2RE and 3RE) improved relative to their parental mAbs (1P, 2P and 3P, respectively) (Table 3).

Pharmacokinetics of the Platform 1 and 3 variants mAbs in cynomolgus monkeys

The SC space varies in composition across species;^{4,6,8} thus, as a means to understand if the SC PK findings in rats were meaningful in another species, we chose to evaluate the PK of a subset of molecules in cynomolgus monkeys since this species is commonly used for predictions of human antibody PK. The PK in cynomolgus monkeys was evaluated following a single

Table 3. Rat pharmacokinetic parameters of the mAbs

Platform	mAb	Route	Dose [^] (mg/kg)	C_{max} (µg/mL)	T_{max} (hr)	AUC_{0-inf} (hr*µg/mL)	CL or CL/F (mL/hr/kg)	$T_{1/2}$ (hr)	k_a [#] (1/hr)	%F
1	1P	IV	1	22.4 ± 3.7	NA	1345.5 ± 252.5	0.62 ± 0.22	163 ± 79	NA	NA
		SC	1	5.0 ± 1.0	96 ± 0	1294.9 ± 134.9	0.78 ± 0.08	133 ± 28	0.009 ± 0.001	108 ± 17
	1RE	IV	1	32 ± 3.8	NA	1513 ± 229	0.37 ± 0.03	96 ± 9	NA	NA
		SC	1	10.0 ± 1	64 ± 37	2176 ± 159	0.3 ± 0.1	221 ± 101	0.021 ± 0.012	144 ± 11
2	2P	IV	1	10.6 ± 1.3	NA	210 ± 52	4.5 ± 0.98	117 ± 9	NA	NA
		SC	1	0.2 ± 0	72 ± 72	39 ± 25	6.4 ± 7.0	1375.2 ± 1550.0	0.036 ± 0.006	25 ± 4 ^a
	2RE	IV	1	21.7 ± 0.8	NA	928 ± 49	0.97 ± 0.07	108 ± 9	NA	NA
		SC	1	3.0 ± 0.3	104 ± 55	564 ± 152	1.5 ± 0.8	158 ± 81	0.012 ± 0.003	61 ± 16
3	3P	IV	1	36.9 ± 1.7	NA	2088 ± 224	0.48 ± 0.06	129 ± 14.2	NA	NA
		SC	1	3.0 ± 1.0	104 ± 60	699 ± 168	0.1 ± 0.2	210 ± 62	0.038 ± 0.016	33 ± 8
	3RE	IV	1	47.5 ± 6.8	NA	3200 ± 121	0.21 ± 0.04	174 ± 21	NA	NA
		SC	1	9.5 ± 1.0	120 ± 0	1816 ± 490	0.5 ± 0.2	154 ± 32	0.013 ± 0.004	57 ± 17

C_{max} , maximal observed serum concentration; T_{max} , time of maximal observed serum concentration; AUC_{0-inf} , area under the serum concentration curve from time zero extrapolated to infinite time; CL, clearance following IV administration; CL/F, apparent clearance as a function of bioavailability following SC administration; $T_{1/2}$, elimination half-life; k_a , rate of SC absorption; %F, SC bioavailability. All PK parameters were determined from non-compartmental pharmacokinetic analyses unless otherwise noted.

^aDetermined from two compartment pharmacokinetic analyses.

NA = not applicable. [^]N = 3/timepoint with serial sampling unless otherwise noted. N = 2 for %F reporting only (standard deviation for illustrative purposes only).

1 mg/kg IV or SC administration of Platform 1 and 3 mAbs. The Platform 2 molecules were not evaluated due to the known cross-reactivity of the molecules in this group with a cynomolgus monkey target, which leads to non-linear clearance following IV administration (data not shown), and would likely confound the interpretation of SC PK. The PK parameters following a single 1 mg/kg IV or SC administration of the Platform 1 and 3 mAbs are reported in Table 4. Overall, the apparent clearance (CL/F) (and intrinsic clearance in the case of the IV administration), rate of SC absorption (k_a) and SC bioavailability of the re-engineered mAbs in each platform (1RE and 3RE) improved relative to their parental mAbs (1P and 3P, respectively) (Table 4).

Evaluations of the relative SC tissue association for Platform 1 and 3 variants mAbs in cynomolgus monkeys

The PK studies suggested a reduction in the amount of the parental mAbs 1P and 3P absorbed into the systemic circulation following SC administration relative to their re-engineered counterparts, mAbs 1RE and 3RE, respectively. As a means to begin to dissect if the lower extent and rate of absorption of the parental mAbs were due to increased residence time within the SC injection site, we assessed the exposure of SC tissue association at the injection site at 6 h post administration for the Platform 1 and 3 molecules in cynomolgus monkeys (Figure 1). The tissue association for the Platform 1 mAbs shows ~30% increased retention of the parent mAb 1P within the SC tissue at 6 h post-dose relative to the re-engineered mAb 1RE (Figure 1). In the case of Platform 3, the parent mAb 3P has an ~2-fold (~50%) increased retention/association at 6 h post SC administration compared to the re-engineered mAb 3RE (Figure 1). Relative to the re-engineered mAbs 1RE and 3RE, the counterpart parental mAbs 1P and 3P, respectively, had shown reduced SC bioavailability and decreased k_a values. Taken together with the SC tissue association findings, the data indicate increased SC tissue association at the injection site reduces mAb exposure.

Evaluations of the relationships between the PK parameters and physiochemical properties

Analysis of the relationship of a subset of the PK parameters (C_{max} , k_a , T_{max} , CL or CL/F and %F) and a subset of the physiochemical properties (HIP, HpnIP, T_{agg} and $T_{m\ on\ set}$) following SC administration to rat or cynomolgus monkey

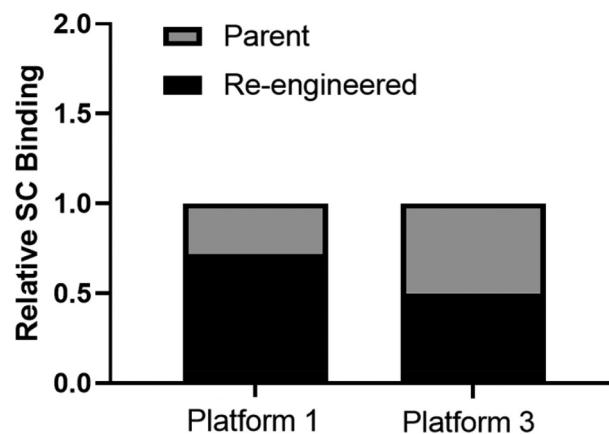


Figure 1. Subcutaneous tissue association of the Platform 1 and 3 parent and re-engineered molecules following a single administration of 0.1 mg/kg of each ^{125}I labeled mAb. Data show the relative SC tissue association of each re-engineered mAb relative to their respective parental mAb. The 1-h post dose time point skin punctures radioactive count for each mAb was considered 100% bound for data normalization purposes. The 6-h post dose collected radioactivity data were compared reported as a fraction of the percent bound relative to the 1-h post dose time point for calculation, data processing and loss of mAb from the SC site reporting over time. Data are the average of two independent SC tissue assessment from two cynomolgus monkeys for each mAb.

are shown in Figures 2 and 3, respectively (IV administration data for PK parameter and physiochemical properties for rat and cynomolgus monkey are in Supplemental Figures 1 and 2, respectively). Since the PK of the Platform 2 molecules was not assessed due to TMDD in cynomolgus monkeys, the analyses included only the Platform 1 and 3 molecules for this species. Tables 5–8 show a summary of the PK and physiochemical correlation findings in rats and cynomolgus monkeys, respectively, following IV and SC administration.

The findings for the IV and SC administration in rats indicate a high correlation (correlation coefficient $r^2 > 0.71$) of IV CL and SC CL/F with both HIP and HpnIP. These correlations, however, were much more variable in cynomolgus monkeys, which may in part be due to the limited number of data points (Tables 5–8). With the exception of the high correlation between HIP and SC k_a in cynomolgus monkeys, the HIP and HpnIP factors did not show any overt correlation with SC k_a , SC C_{max} or SC %F across species (Tables 5–8). High and medium (correlation coefficient r^2 between 0.51 and 0.71) correlations were observed between SC k_a and $T_{m\ on\ set}$, as well as, SC C_{max} and T_{agg} in both species. In terms of SC %F, in cynomolgus monkeys there was a high correlation observed

Table 4. Cynomolgus monkey pharmacokinetic parameters of the mAbs

Platform	mAb	Route	Dose [^] (mg/kg)	C_{max} (μ g/mL)	T_{max} (hr)	$AUC_{0-\infty}$ ($hr \cdot \mu$ g/mL)	CL or CL/F (mL/hr/kg)	$T_{1/2}$ (hr)	k_a [#] (1/hr)	%F
1	1P	IV	1	24.0 \pm 0.6	NA	2910 \pm 587	0.35 \pm 0.08	278 \pm 76	NA	NA
		SC	1	4.0 \pm 0.7	48 \pm 24	1492 \pm 201	0.68 \pm 0.10	248 \pm 23	0.033 \pm 0.006	51 \pm 7
	1RE	IV	1	26.9 \pm 2.4	NA	4264 \pm 1242	0.25 \pm 0.06	382 \pm 162	NA	NA
		SC	1	12.6 \pm 2.6	24 \pm 0	3187 \pm 111	0.31 \pm 0.01	235 \pm 53	0.021 \pm 0.003	75 \pm 3
3	3P	IV	1	27 \pm 1.3	0.17 \pm 0.12	1832 \pm 231	0.56 \pm 0.7	271.8 \pm 55.9	NA	NA
		SC	1	3.4 \pm 1.3	60 \pm 17	837 \pm 452	1.4 \pm 0.8	214.5 \pm 102.9	0.094 \pm 0.002	46 \pm 6
	3RE	IV	1	25.54 \pm 3.6	NA	3473 \pm 2048	0.35 \pm 0.21	213.2 \pm 141.2	NA	NA
		SC	1	7.92 \pm 0.4	132 \pm 50.9	3907 \pm 2406	0.32 \pm 0.19	337.8 \pm 48.2	0.049 \pm 0.003	100 ^a \pm 8

C_{max} , maximal observed serum concentration; T_{max} , time of maximal observed serum concentration; $AUC_{0-\infty}$, area under the serum concentration curve from time zero extrapolated to infinite time; CL, clearance following IV administration; CL/F, apparent clearance as a function of bioavailability following SC administration; $T_{1/2}$, elimination half-life; k_a , rate of SC absorption; %F, SC bioavailability. NA = not applicable. [^]N = 3 cynomolgus monkeys/time point. All PK parameters were determined from non-compartmental pharmacokinetic analyses unless otherwise noted.

^aDetermined from two compartment pharmacokinetic analyses.

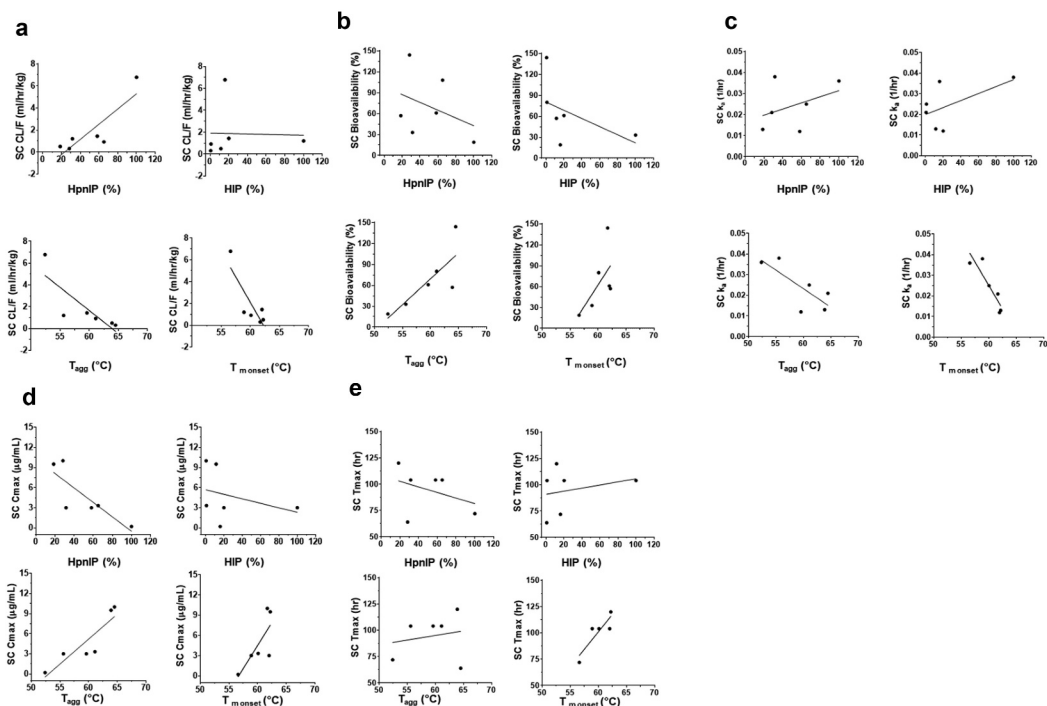


Figure 2. Correlation plots of the rat pharmacokinetic parameters following SC administration of mAbs 1P and 1RE in Platform 1, mAbs 2P and 2RE in Platform 2 and mAbs 3P and 3RE in Platform 3. Correlation plots for the (a) CL/F, (b) SC bioavailability, (c) rate of SC absorption (k_a), (d) C_{max} and (e) T_{max} with the physicochemical properties HpnlP, HIP, T_{agg} and $T_{m\ onset}$.

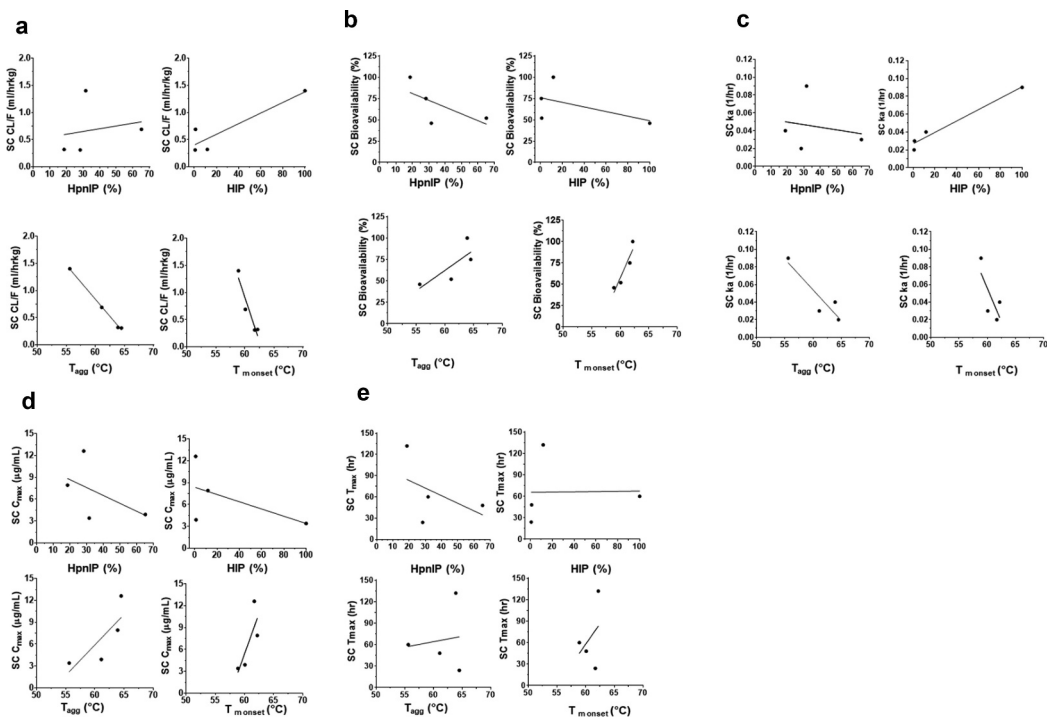


Figure 3. Correlation plots of the cynomolgus monkey pharmacokinetic parameters following SC administration of mAbs 1P and 1RE in Platform 1 and mAbs 3P and 3RE in Platform 3. Correlation plots for the (a) CL/F, (b) SC bioavailability, (c) rate of SC absorption (k_a), (d) C_{max} and (e) T_{max} with the physicochemical properties HpnlP, HIP, T_{agg} and $T_{m\ onset}$.

Table 5. Correlation scores for the relationship of the physiochemical parameters with the PK of the mAbs assessed following a single IV administration to rats^a

Physiochemical parameter	PK parameter			
	IV C _{max}	IV AUC _{0-∞}	IV clearance	IV T _{1/2}
HpnIP	High	High	High	Low
HIP	High	High	High	Low
T _{agg}	Low	Low	Medium	Medium
T _{m onset}	Low	Low	Medium	Low

^aCorrelation score rankings of high, medium, and low are defined by data from the determination of the correlation coefficient values (r^2) derived from the linear regression best line fit of each physiochemical parameter with each PK parameter. High r^2 values ranged from 0.71- to 1.0. Medium r^2 values ranged from 0.51 to 0.70. Low r^2 values were <0.50.

with T_{m onset} and medium correlation with T_{agg} in both species. Overall, the findings suggest a connectivity of mAb physiochemical properties with PK.

Discussion

Many mAb-based biopharmaceuticals are delivered via SC injection. Optimizing the *in vivo* SC PK of mAbs to improve their drug-ability is thus an area of considerable attention for therapeutic antibody engineering. In this study, we directly examined the interplay between multiple mAb physiochemical factors (charge, hydrophobicity, aggregation potential and thermal stability) on the rate and extent of SC absorption of six and four humanized mAbs in rats and cynomolgus monkeys, respectively, as a means to dissect parameters affecting SC PK. There are several factors that have been clearly shown to influence the kinetics of a mAb *in vivo*. These include attributes of the therapeutic target (membrane bound or soluble, density, turnover) and the biochemical properties of the antibody (i.e., physiochemical properties, antigen affinity, glycosylation, charge, proteolytic stability; FcRn interactions).^{12,15,18,21-24} Herein, the clearance of these molecules was not a consequence of target interactions (TMDD) since the kinetics of the mAbs were assessed in a species (rat, cynomolgus monkey or both) in which there were insignificant concentrations of antigen present to influence the clearance. The PK was also unrelated to aberrant FcRn binding because the mAbs showed receptor binding affinities at pH 6 in the range reported for molecules with well-behaved kinetics and no direct FcRn interactions at neutral pH (Table 2). Thus, the focus was on understanding the role of the aforementioned physiochemical parameters in the context of the SC space/anatomy and

Table 7. Correlation scores for the relationship of the physiochemical parameters with the PK of the mAbs assessed following a single IV administration to cynomolgus monkeys^a

Physiochemical parameter	PK parameter			
	IV C _{max}	IV AUC _{0-∞}	IV clearance	IV T _{1/2}
HpnIP	Medium	Low	Low	Low
HIP	Medium	Low	Low	Low
T _{agg}	Low	High	High	Low
T _{m onset}	Low	High	High	Low

^aCorrelation score rankings of high, medium, and low are defined by data from the determination of the correlation coefficient values (r^2) derived from the linear regression best line fit of each physiochemical parameter with each PK parameter. High r^2 values ranged from 0.71- to 1.0. Medium r^2 values ranged from 0.51 to 0.70. Low r^2 values were <0.50.

composition. Importantly, using this approach we demonstrated that several physiochemical properties are critical with regard to their influence on mAb kinetics following SC administration and that some of these (e.g., T_{m onset} and T_{agg}) are unique with regard to having increased connectivity with SC relative to IV administration across species.

The reduced SC bioavailability, slowed rate of SC absorption and increased clearance of parent mAbs across the three platforms relative to their re-engineered counterparts in rats and cynomolgus monkeys that we observed suggest that altering inherent mAb charge, hydrophobicity, aggregation potential and thermal stability via antibody engineering may lead to improved *in vivo* SC absorption rate and bioavailability. The relative contribution of each of these factors underlies the basic *in vivo* characteristics of an antibody and heavily influences strategies aimed at optimizing the PK properties mAbs. While there has been progress toward understanding each of these aspects individually (especially following IV administration to preclinical species), few studies report the integrated influence of multiple mAb physiochemical factors, including thermal, chemical and physical on the SC absorption and bioavailability of mAbs.^{12,15,18,21-24} In our study, the combination of high local positive charge (as measured by heparin interactions), increased hydrophobic interaction potential and low thermal stability leading to increased aggregation potential had the largest negative magnitude of effect on the rate of SC absorption, apparent clearance and bioavailability as evident from the PK findings for mAb 2P in rats compared to the other antibodies within and across Platforms. These factors thus should be considered for improved *in vivo* performance following SC administration. Given the increased compliance and convenience benefits of SC administration for patients, dissecting

Table 6. Correlation scores for the relationship of the physiochemical parameters with the PK of the mAbs assessed following a single SC administration to rats^a

Physiochemical parameter	PK parameter						
	SC C _{max}	SC T _{max}	SC AUC _{0-∞}	SC CL/F	SC T _{1/2}	SC k _a	SC %F
HpnIP	Medium	Low	Medium	High	Medium	Low	Low
HIP	Medium	Low	Medium	High	Medium	Low	Low
T _{agg}	High	Low	High	Medium	Medium	Medium	Medium
T _{m onset}	Medium	Low	Medium	Medium	Medium	High	Low

^aCorrelation score rankings of high, medium, and low are defined by data from the determination of the correlation coefficient values (r^2) derived from the linear regression best line fit of each physiochemical parameter with each PK parameter. High r^2 values ranged from 0.71- to 1.0. Medium r^2 values ranged from 0.51 to 0.70. Low r^2 values were <0.50.

Table 8. Correlation scores for the relationship of the physiochemical parameters with the PK of the mAbs assessed following a single SC administration to cynomolgus monkeys^a

Physiochemical parameter	PK parameter						
	SC C_{max}	SC T_{max}	SC $AUC_{0-\infty}$	SC CL/F	SC $T_{1/2}$	SC k_a	SC %F
HpnIP	Low	Low	Low	Low	Low	Low	Low
HIP	Low	Medium	Low	High	Medium	High	Low
T_{agg}	Medium	Low	High	High	Low	High	Medium
$T_{m\ onset}$	Medium	Low	High	High	Medium	Medium	High

^aCorrelation score rankings of high, medium and low are defined by data from the determination of the correlation coefficient values (r^2) derived from the linear regression best line fit of each physiochemical parameter with each PK parameter. High r^2 values ranged from 0.71- to 1.0. Medium r^2 values ranged from 0.51 to 0.70. Low r^2 values were <0.50.

factors influencing the SC disposition of mAbs will further extend the drug-ability of mAb-based therapeutics and improve patient outcomes and experience.

Considerable insight was gained from the comparison of the physiochemical characterization of the mAbs with regard to global (pI and zeta potential) and local surface charge (HpnIP value) assessment. Some similarities and a number of differences in the sensitivity of the local and global charge findings across the three Platforms were observed in this comparison. In our studies for the global assessment of mAb surface charge, the pI values of the mAbs ranged from 8.2 to 9.4; however, within a Platform, the pI values were similar and showed no more than a marginal 0.3 pI unit shift. This was the case even for molecule pairs in each Platform that showed >2-fold differences in HpnIP values, which gives additional insight into the assessment of local surface charge being a more sensitive measure of potential charge-based interactions than the pI. It is worth noting that, given the overall large molecular weight of mAbs, the few residues altered across mAbs within a Platform (no more than 5 residues changes between mAbs) and well-ordered tertiary structure of antibodies, the modest changes in a global measure of charge, such as pI, within a given Platform may not be unexpected. Similar to the pI observation, changes in zeta potential (which is also a global measure of charge) across the molecules were also marginal, and thus indicated similar overall or global surface net charge of the mAbs. These global assessments of surface charge were difficult to fully interpret/connect with the SC PK findings. Previous reports have suggested some mixed finding with regard to the value of assessing pI or other global measures of mAb surface charge and their connectivity to mAb kinetics. Both Li and coworkers and Igawa *et al.* have demonstrated that lowering the pI by ~1 unit or more (overall range of 6.1 to 9.2 across studies) slows IgG clearance.^{25,26}

In contrast to these findings, our lab has reported the influence of subtle modifications of molecular charge without affecting pI as increasingly connected to the PK of IgGs compared to global assessments.¹⁹ Along these lines, Sampei *et al.* found modulating a positive charge patch with the addition of a single acidic residue on an anti-FIXa antibody resulted in decreased clearance of the molecule. While they did not report whether pI changes were also observed, it is reasonable to speculate that changing a single residue in the context of a ~ 150 kDa mAb is unlikely to significantly modulate the global charge.²⁷ Combined, these studies suggest reducing the overall net positive molecular charge either globally or locally

improves mAb PK via decreased nonspecific cellular interactions that, in part, may enhance intracellular IgG uptake and/or rate of degradation.

Here, we report that the largest difference in charge-based interactions within and across mAb Platforms was observed with HpnIP, which is more sensitive in detecting local charge patches compared to global surface charge assessments (i.e., pI or zeta potential measures). All the molecules showed some level of charge-based interaction in the heparin column interaction assay indicative of the potential to have nonspecific binding (NSB) for negatively charged *in vivo* matrices such as the SC space. The reported findings indicate that the local position of charge display (i.e., in a solvent-accessible area such as the CDR) is an impactful aspect that may be under-represented in the overall pI or zeta potential determination and better characterized via HpnIP when considering mAb engineering approaches for PK connectivity attributes.

In addition to the component of charge-based driven NSB potential influencing PK, the physiochemical characterization for the three mAb Platforms indicates the potential for hydrophobic interactions to also affect kinetics. These may be more important in the context of *in vivo* interactions within the SC space where compositionally there are fat lobules, adipocytes, collagen, and other connective tissues, which likely favor non-covalent hydrophobic interactions. Platforms 2 and 3 (HIP range of ~16–100%) had much larger inherent HIP than Platform 1 (HIP values of ~1%), suggesting the potential for a combination of both charge- and hydrophobic-related interactions with varying degrees affecting the *in vivo* performance of these molecules. Interestingly, the inherent differences in hydrophobic-based interactions showed some connectivity with the onset of thermally induced tertiary structure unfolding and aggregation potential across the three mAb Platforms. The genesis of this observation is the aggregation onset (T_{agg}) across the three Platforms presented here. In the case of the Platform 1 mAbs, the T_{agg} of mAb 1P (parent with reduced SC %F) and 1RE (re-engineered mAb with higher SC %F) are comparable; these mAbs predominantly show differences in their charge compared to hydrophobic-based interactions. In contrast, the T_{agg} is improved for both the Platform 2 mAbs 2P and 2RE (from 52.4°C to 59.6°C, respectively) and Platform 3 mAbs 3P and 3RE (from 55.6°C to 63.9°C, respectively); however, unlike the Platform 1 mAbs, the Platform 2 and 3 molecules displayed increasing differences in their hydrophobic compared to charge-based interactions. The improved T_{agg} observed in Platform 2 with mAb 2RE relative to mAb 2P, as

well as in Platform 3 with the relative rank order of T_{agg} improvement of mAb 3RE > mAb 3P combined, indicate molecules with increased HIP are more sensitive to unfolding. This may be due to a propensity for attempting to bury solvent-accessible hydrophobic regions through a greater inclination to change conformation via unfolding, and thereby result in increased aggregation. The reduction in surface hydrophobicity led to a reduced tendency to aggregate as measured by T_{agg} . The comparable T_{agg} of the Platform 1 mAbs, which were predominately influenced by charge-based interactions (as observed in HpnIP) that typically behave in a repulsive manner with regard to self-association or aggregation, also support this hypothesis.

The Platform 1 mAbs were reasonable surrogates for predominantly studying the effect of local charge-related NSB on SC absorption and bioavailability given these molecules showed strong charge-based binding signals and little/no hydrophobic interaction potential (values in the single digit percentage range) *in vitro*. Since the SC space consists of a milieu of negatively charged GAGs and other proteoglycans, the reduced k_a and SC bioavailability of the more solvent-exposed positive charge parental mAb 1P in both rats and cynomolgus monkeys suggests a mechanism whereby mAb 1P has enhanced residence within the SC space, which reduces the rate and extent of mAb 1P being absorbed into the blood circulation compared with the re-engineered lower HpnIP mAb 1RE. This hypothesis is also supported by the observed increased SC tissue association of mAb 1P observed in cynomolgus monkey relative to mAb 1RE (Figure 1). We speculate reducing the local charge-related HpnIP lowered the NSB SC tissue matrix interaction of mAb 1RE relative to mAb 1P, which improved the *in vivo* PK of mAb 1RE. Under the conditions leveraged in this study, the temperatures at which the onset thermal instability and aggregation occurred for the two mAbs was marginally dissimilar with mAb 1RE (re-engineered molecule) showing slightly lower values in both aspects than mAb 1P. The data suggest for molecules with little/no hydrophobic interaction potential, but high local charge-related physiochemical aspects, thermal instability and aggregation are not distinguishing factors. The improved SC absorption and bioavailability for mAb 1RE are likely related to reduced nonspecific tissue uptake and subsequent catabolism compared to mAb 1P, which is supported by earlier studies showing enhanced NSB-driven cellular association/binding led to mAb degradation.¹⁹ Interestingly, while the relative rank order of the SC PK of mAb 1RE and mAb 1P were the same in cynomolgus monkeys and rats, differences in the magnitude of k_a and bioavailability were observed across species. This may be related to the known differences in the compositional preponderance of the components within SC tissue matrix across species; these SC tissue compositional differences across species may also affect the correlation analyses across species (Figures 2 and 3). Nonetheless, while the magnitude of the effects may not be fully predictable across species because of the differences in SC tissue architecture, the nonspecific nature of the charge-based interactions strongly suggests similar findings would be anticipated in humans.

In contrast to the Platform 1, Platforms 2 and 3 facilitated dissection/connectivity of the impact of varying levels of both

charge-related NSB and hydrophobic-related interactions on SC absorption and bioavailability. The Platform 2 mAb pair served as a reasonable set of molecules to dissect the role of charge-based interactions (mAb 2P shows ~2-fold higher HpnIP than mAb 2RE) with an underlying similar hydrophobic interaction component (mAbs 2P and 2RE have HIP values of ~16% and ~20%, respectively). The charge re-engineering improved the kinetics (i.e., clearance) and SC absorption/bioavailability of mAb 2RE compared to mAb 2P by ~4.5-fold and ~3-fold, respectively, in rats. Thus, similar to Platform 1 findings, the Platform 2 data also support positive charge-based interactions negatively affect SC absorption/bioavailability, likely through increased binding/association with the components of SC tissue matrix. However, it is important to note that although charge rebalancing significantly improved the PK, mAb 2RE still displays a relative clearance rate and SC bioavailability of ~1 mL/hr/kg and ~60%, respectively, in rats. The engineered mAb 2RE is actually kinetically inferior to the charge-unbalanced parent mAb 1P (CL/F and SC %F of ~0.8 mL/hg/kg and ~70%, respectively) even though mAbs 1P and mAb 2RE have similar HpnIP values. The major differences between the mAb 1P and the mAb 2RE variants are in their HIP values, which show mAb 2RE has an ~20-fold higher hydrophobic interaction potential than mAb 1P. Taken together, the data suggest that the hydrophobic interaction potentials for the Platform 2 mAbs are an important component of NSB influencing both mAbs 2P and 2RE clearance, SC absorption and bioavailability. The data suggest further engineering to reduce the HIP of mAbs 2P and 2RE would likely improve their SC absorption through reduced interactions with the SC tissue matrix.

Similar to Platform 2, the Platform 3 mAbs were also insightful for dissecting the role of hydrophobic interactions on the rate and extent of mAb SC absorption and bioavailability. Platform 3 is unique from Platform 2 in that the mAbs in Platform 3 show larger differences in the hydrophobic interactions (~9-fold reduction in mAb 3RE HIP relative to mAb 3P whereas the Platform 2 mAbs have comparable HIP values) and some charge-based interactions in a more moderate range (HpnIP values of ~20–32% for mAbs 3P and 3RE compared to >55% for mAbs 2P and 2RE). Thus, while not fully seamless with regard to HIP and HpnIP, Platform 3 does directionally facilitate the interrogation of hydrophobicity with a more modest influence from charge than the other two Platforms. The ~9-fold higher HIP value for mAb 3P compared to mAb 3RE1 was connected to an ~1.6-fold more rapid clearance and ~2-fold lower bioavailability of mAb 3P than mAb 3RE1 in cynomolgus monkeys, respectively, and an ~2.3-fold more rapid clearance and ~1.7-fold lower bioavailability of mAb 3P compared to mAb 3RE1 in rats, respectively. Thus, the Platform 3 data indicates that reducing the hydrophobic interactions was beneficial to the PK, but, compared to the PK enhancements observed for Platform 2 (~4.5-fold and ~3-fold improvements in clearance and SC bioavailability, respectively), the Platform 3 improvements were more modest. The findings suggest that for the molecules herein, when both charge and hydrophobicity interactions are present, reducing charge-based interactions may have a greater effect on enhancing kinetics than reducing hydrophobic interactions. Notably,

the high correlation across Platforms between the slow clearance (or CL/F for SC route) and reduced HIP, as well as decreased HpnIP for both the IV and SC administration, does indicate reducing hydrophobic interactions or charge-based association will improve PK for both parenteral routes across species; thus, it is important to optimize molecules for both these properties. Furthermore dissection of the C_{max} across Platforms suggests SC route-specific high correlations with T_{agg} and $T_{m\ onset}$. This may be related to thermal stability playing an increased role within the SC tissue matrix prior to absorption into the blood circulation (Figures 2 and 3). A high correlation was generally not consistently observed across rats and cynomolgus monkeys between k_a or SC bioavailability and the majority of the physiochemical properties (with the exception of $T_{m\ onset}$ and k_a) across Platforms. This, in part, may be due to the limited number of mAbs examined. Despite the number of examples reported, the reasonable connectivity of some of these parameters indicates further studies with additional molecules are warranted to better delineate these relationships both within and across species. These follow-up interrogations could also include additional IgG isotype evaluations.

Our findings suggest mAb variants that have an increased rate of SC absorption and bioavailability have reduced local positive charge, potentially lower hydrophobic matrix interactions, higher thermal stability and reduced thermally induced aggregation potential. These observations led us to hypothesize that the results may be related to three mechanisms: 1) decreased SC tissue matrix interactions due to charge repulsion with the negatively charged components of the SC milieu, including constituents of the ECM (e.g., GAGs); 2) decreased SC tissue component interactions due to reduced hydrophobic-based van der Waals interactions with adipose tissues; and 3) reduced potential for local and global unfolding due to physiologically relevant temperatures, which may lead to increased recognition by macrophage-based host defense mechanisms in the SC space. The reduced clearance of mAbs 1RE, 2RE and 3RE (relative to mAbs 1P, 2P and 3P, respectively) is likely a consequence of these mechanisms, but to variable degrees. In particular, the reduced SC absorption and bioavailability of mAbs 1P and 3P correlate well with the high degree of local SC tissue association and subsequent degradation due to a combination of increased charge- or hydrophobic-based interactions, respectively. Although tissue binding data were not assessed for the Platform 2 molecules due to TMDD in cynomolgus monkeys, we speculate that for mAb 2P the preponderance of data suggest a likely increased degree of local SC tissue binding due to both charge and hydrophobic interactions.

From a conceptual perspective, SC-administered, kinetically poorer mAbs likely bind GAGs, fat lobules and cells (adipocytes and endothelia) nonspecifically to a greater extent than molecules without these properties. As a result, the greater degree/strength of association with SC tissue components does not allow the mAbs to be taken into the lymphatic system for subsequent release into the peripheral circulation. In addition, increasing endothelial cellular association with membrane components may lead to the mAb's increased cellular uptake, but lack of ability to be effectively salvaged from intracellular

degradation. Due to the nonspecific nature of the interactions, this may partition the mAbs with solvent-exposed charge and increased hydrophobic potential properties away from the recycling pathway and toward lysosomal degradation. Lastly, local tissue interactions and sensitivity to the higher physiological temperatures *in vivo* may be facilitating some loss of tertiary structure for some molecules, which leads to some increased aggregation potential. These aggregates may appear 'foreign' to the system and facilitate an increased response by SC macrophages to facilitate removal (i.e., degradation) of the mAbs, so that these are no longer available for absorption. This seems to make sense if one considers both the preponderance physiochemical findings in the context of the potential cellular and SC tissue matrix interactions as discussed above.

In summary, the data in this report suggest there are many mAb-based and SC matrix-centric factors to consider when using antibody engineering or screening approaches to improve the SC bioavailability/drug-ability of mAb biotherapeutics. Applying a rationally based approach to integrate the complexities of these factors can affect the *in vivo* performance of mAbs. Since additional characteristics of both the mAb and formulation (chemical stability, FcRn binding, solubility, concentrate-ability) can influence the SC disposition and elimination, it will be impactful to investigate the relative roles of these additional mechanisms to ultimately design, engineer and screen molecules with increased therapeutic value and drug-ability.

Materials and methods

Construction, expression, and purification of the six mAbs

The Fab regions were discovered and engineered at Eli Lilly and Company. These were cloned into mAb expression vectors to fuse with constant regions of human kappa light chain and either a human IgG₁ or IgG₄ heavy chain using standard molecular biology approaches and confirmed by DNA sequencing. All the IgGs were expressed using a CHO expression system. The mAbs were purified from culture supernatants using standard Protein-A Sepharose (GE Healthcare) affinity chromatography followed by size exclusion chromatography methods described previously.¹⁹

Evaluation of the cynomolgus monkey FcRn binding affinity

Recombinant soluble cFcRn was expressed in 293EBNA cells transfected with plasmids encoding for the soluble portion of α FcRn and β_2 -microglobulin, and the protein was purified as described previously.^{28,29} The interaction of the IgG₁ and IgG₄ molecules with recombinant, immobilized cFcRn were monitored by SPR detection using a Biacore 3000 instrument (GE Healthcare) as described previously.^{28,29} Briefly, recombinant soluble cFcRn was immobilized to flow cell 2 of a CM5 sensor chip using amine coupling chemistry (GE Healthcare). The cFcRn immobilization surface density was approximately 300 RU. The first flow cell was used as a blank control surface lacking cFcRn. All binding experiments were performed with compounds dissolved in running buffer

phosphate-buffered saline (PBS) with 0.005% Tween 20, pH 6 or PBS with 0.005% Tween 20, pH 7.4 and the samples were run at a flow rate of 100 $\mu\text{l}/\text{min}$ for 30 seconds with a dissociation time of 10 minutes. PBS (pH 7.4) was used as dissociation buffer. PBS with 0.005% Tween 20, pH 6 was used as running buffer for the experiments performed to determine the affinity of IgGs to cFcRn. A concentration range of 0.00316 μM to 3.16 μM of each of the IgGs was used to estimate the association and dissociation constants. The binding data were obtained by subtracting the signal of flow cell 1 (blank flow cell not coupled with FcRn) from flow cell 2. Kinetic (association and dissociation) data were then simultaneously fit to a heterogeneous binding model for IgG-cFcRn interactions (BIAevaluation, Ver. 4.1). The data curves for binding and dissociation phases of the sensorgrams for the IgGs at pH 6.0 had low residuals and low χ^2 values. The mean of K_d values accounting for the greatest fraction of binding from two independent experiments were reported.

Evaluation of mAb isoelectric points

Capillary isoelectric focusing (cIEF) was used to measure the pI of all mAbs. All protein samples were diluted to 1 mg/mL with 10 mM citrate at pH 6. The final protein concentration was diluted to 0.25 mg/mL by the cIEF master solution, which includes 4% pH 3–10 pharmalyte and 4 M urea. Maurice[®] (Protein Simple, San Jose, CA) was used for data acquisition and analysis, which were achieved through the Compass for iCE software (Version: 1.1.5 Build ID: 0920). During the data acquisition, the markers of 4.1 and 9.5 were used and separation of various charged species were done by applying 1500 volts for 1 minute followed by 3000 volts for 9 minutes. After acquisition, the raw data were processed by correct the marker position. The peak with the highest intensity and area within the chromatogram was assigned as the pI value of the protein.

Zeta potentials of 1 mg/mL mAb solutions in either 10 mM histidine pH6 or 10 mM acetate pH5 were measured by electrophoretic light scattering with a Zetasizer[®] (Malvern Instruments Ltd., UK) instrument. At 25°C, the particle refractive index was set at 1.003. Solution refractive index, viscosity, and dielectric constant were calculated based on the solution components using Zetasizer software.

Evaluation of temperature of melting or midpoint of temperature transition (T_m) and the onset temperature of tertiary structure unfolding

A MicroCal VP-Capillary DSC system (Malvern Instruments Ltd., Malvern UK) was used for midpoint of temperature transition (T_m) measurement. Samples were diluted to 1 mg/mL before measurement. The thermograms were generated by scanning the temperature from 20°C to 105°C at a rate of 1°C/min and 60 psi constant pressure was applied during measurement. Four placebo pairs were run before protein samples to generate clean baseline. MicroCal VP-Capillary DSC Automated Analysis software 2.0 was used for data analysis. The T_m onset was defined as the temperature where specific heat (C_p) reached 2% of the maximum peak value. Each protein

sample was also manually fitted to a non-2 state model to calculate T_m values. During the model fitting, peaks were visually selected and fitted until chi square values did not change.

Fluorescence coupled with static light scattering was used to evaluate the onset temperature of tertiary structure unfolding. A UNit[®] (Unchained labs, Pleasanton, CA) system was used to measure the fluorescence and static light scattering simultaneously. During the measurement, ~8.8 μL protein sample at 1 mg/mL was loaded to the cuvette; the samples were held at 20°C for 120 s and then ramped to 95°C at the rate of 0.3°C/min. Both fluorescence and static light scattering (at 266 nm) were collected after excitation at 266 nm. After measurement, the data were loaded onto the UNit[®] analysis software, the raw fluorescence signals were extracted and further processed with excel. The onset of tertiary structure unfolding (T_{onset}) was defined as the temperature when center of mass (CM) of the fluorescence emission spectrum ($\lambda_m = \sum_{\lambda} f_{\lambda} \lambda / \sum_{\lambda} f_{\lambda}$) is increased by 0.4% compared to the initial value (the average of the first 5 points). The raw SLS data were analyzed by the UNit[®] analysis software, where the onset of aggregation (T_{agg}) is defined as the first temperature at which the first derivative is larger than 0.

Heparin column binding and hydrophobic interaction column binding

HiTrap Heparin HP Sepharose (GE Healthcare) with a 1 mL capacity and an Agilent 1100 (Santa Clara, CA) system were used for evaluating the relative heparin-binding affinity of the mAbs. In the experiment, 40 μg proteins were injected to the column and eluted using a linear gradient of 0 to 1 M NaCl at 20 mM potassium phosphate, pH 7.0 with 214 nm UV detector and the flow rate was 1 mL/min.

The Tosho NPR Butyl column (San Francisco, CA) and an Agilent 1100 (Santa Clara, CA) system were used to evaluate the relative hydrophobic interaction potential of the mAbs. Stock solutions of each mAb were diluted to 0.5 mg/mL with 50 mM potassium phosphate, pH 6.7, 1 M ammonium sulfate. In the experiment, 5 μg proteins were injected to the column and eluted using a linear gradient of 1 to 0 M ammonium sulfate at 50 mM potassium phosphate, pH 6.7 with 214 nm UV detector and the flow rate was 0.5 mL/min.

The elution time of each sample was recorded to evaluate the relative heparin interaction potential (HpnIP%) or hydrophobicity interaction potential (HIP%):

$$\text{HpnIP\%orHIP\%} = \frac{T_i - T_o}{T_e - T_o} \times 100 \quad 1$$

where T_i is the elution time of sample, T_o is the column equilibrium time before the gradient, T_e is the time for the end of the gradient.

Sprague Dawley rat pharmacokinetic studies

Sprague Dawley rats were obtained from The Jackson Laboratory (Bar Harbor, ME). All rats were treatment-naive males between the ages of 8 to 11 weeks with an average weight

of 0.3 kg (\pm 0.05 kg). PK studies were conducted at Covance (Madison, WI) and were designed and executed within accordance of the Animal Use Protocol (AUP) and adherence to the Covance Institutional Animal Care and Use Committee (IACUC) regulations. The mAbs were dosed both IV and SC at 1 mg/kg with a dose volume of 1 mL/kg (dose prepared in PBS pH 7.4). A dose of 1 mg/kg was selected as no TMDD was expected in the rodents for any of the antibodies. Blood samples were collected from the jugular vein at 0.083, 1, 6, 12, 24, 48, 72, 96, 120, 168, 240 and 336 h after dose administration in replicates of 2 or 3 for each mAb. The blood samples were allowed to clot at ambient temperature prior to centrifugation to obtain serum.

Cynomolgus monkey pharmacokinetic studies

All monkeys were between the ages of 2 to 3 y old with an average weight of 3 kg (\pm 0.5 kg). PK studies were conducted at Covance (Madison, WI) and were designed and executed within accordance of the AUP and adherence to the Covance IACUC regulations. The Platform 1 and 3 mAbs were dosed both IV and SC at 1 or 5 mg/kg with a dose volume of 1 mL/kg (dose prepared in PBS pH 7.4). These doses were selected because there was no TMDD expected in the monkeys for any of the antibodies and anticipated to be in the linear PK range for both platforms allowing for non-target mediated PK parameter estimates across doses and routes. Blood samples were collected from the femoral vein at 1, 6, 12, 24, 48, 72, 96, 168, 240, 336, 432, 504, 600 and 672 h after dose administration in replicates of 2 for each mAb. The blood samples were allowed to clot at ambient temperature prior to centrifugation to obtain serum. Platform 2 was not evaluated in cynomolgus monkeys due to an expected TMDD that would affect PK.

Bioanalytical assays and pharmacokinetic data analysis

Concentrations of the mAbs in Sprague Dawley rats or cynomolgus monkey serum were determined using anti-human IgG or anti-human kappa enzyme linked immunosorbent assays for each of the molecules. In brief, each well of a microtiter plate was coated with either goat anti-human IgG (Jackson ImmunoResearch Laboratories, Inc., West Grove, PA; Catalog Number 109–006–097) or goat anti-human kappa antibody (Southern Biotech, Birmingham, AL; Catalog Number 2060–01). After sample pretreatment of a 1:10 minimum required dilution, washing and blocking, all the standards, control samples, and study samples were added to the plates, then incubated for 1 h at room temperature. After washing, the bound molecules were detected with a horseradish peroxidase-conjugated mouse anti-human IgG (Fc) antibody (Southern Biotech, Birmingham, AL; Catalog Number 9040–05) via TMB Microwell Peroxidase Substrate System (KPL, Gaithersburg, MD) for a colorimetric response. Plates were read at 450–493 nm with a reference standard of 630 nm. Concentrations from plasma or serum samples were determined from a standard curve prepared with known amounts of the antibody dosed in the measured samples. The concentration of study samples from each mAb were determined by interpolation from a standard curve using a 4/5- parameter

logistic curve fit with $1/y^2$ response weighting using Watson LIMS software version 7.4 (Thermo Scientific Inc. Waltham, MA USA). The standard curve range for the Platform 1 mAbs ranged from 8 to 500 ng/mL, and the lower limit of quantitation (LLOQ) was defined as 15 ng/mL. The standard curve range for the Platform 2 and 3 mAbs were from 4 to 384 ng/mL, and the LLOQ was defined as 8 ng/mL.

PK parameters were calculated using the WinNonlin Professional (Version 3.2) software package (Pharsight Corporation, Mountain View, CA). Serum concentration-time data were calculated using a model-independent approach based on the statistical moment theory. The parameters calculated included the maximum serum concentration (C_{max}), area under the curve ($AUC_{0-\infty}$), clearance (CL), elimination half-life ($t_{1/2}$) and rate of absorption (k_a).

¹²⁵I-mAb preparation and subcutaneous tissue association quantification in cynomolgus monkeys

The Platform 1 and 3 mAbs were radiolabeled with ¹²⁵I to monitor the percent loss from the subcutaneous site of injection in cynomolgus monkeys. Radio-iodination (¹²⁵I) of mAbs for percent subcutaneous tissue bound calculations was performed using the succinimidyl iodobenzoate (SIB) iodination method. Briefly, 2–3 mCi of Na ¹²⁵I (Perkin-Elmer, Billerica, MA) was reacted with 5–8 μ g N-succinimidyl-3-(tri-n-butylstannyl) benzoate (American Advanced Scientific, College Station, TX) to generate ¹²⁵I SIB, which in turn was reacted with 1–2 mg of each test mAb. The labeled proteins were purified by gel filtration over OD-10 desalting columns (GE Healthcare, Piscataway, NJ) to remove unconjugated ¹²⁵I SIB and protein concentrations verified by UV spectroscopy. Dosing solutions were prepared by mixing unlabeled mAbs with the corresponding ¹²⁵I-mAb to a final concentration of 1 mg/ml in buffer. The radioactive specific activity of the dosing solutions was an average of 0.1 mCi/mg using a tissue puncture sampling approach. Radiochemical purity of dosing solutions was characterized by trichloroacetic acid (Sigma-Aldrich, S. Louis, MO) precipitation and size-exclusion HPLC using an Agilent Bio SEC-3 column (Agilent Technologies, Santa Clara, CA). The percentage of free ¹²⁵I was less than 1% in all dosing solution preparations.

All cynomolgus monkeys were treatment males between the ages of 2 to 3 y old with an average weight of 3 kg (\pm 0.5 kg). Studies conducted at Covance (Madison, WI) and were designed and executed within accordance of the AUP and adherence to the Covance IACUC regulations. The Platform 2 mAbs were not evaluated due to expected TMDD. ¹²⁵I labeled Platform 1 and 3 mAbs were administered SC in the thoracic region at 0.1 mg/kg/site with a dose volume of 300 μ L per site of injection (dose prepared in PBS pH 7.4). Two sets of four monkeys were administered ¹²⁵I labeled mAbs 1P and 1RE or ¹²⁵I labeled mAbs 3P and 3RE each at pre-determined and distinctly isolated injection sites each for antibody for up to six administration sites per animal.

For quantification of the loss of mAb from the SC tissue administration site, each site of ¹²⁵I labeled mAb administration underwent skin punch biopsies of 8 mm at a specified post dose time. One skin punch biopsy represented one site of

administration at a pre-determined post dose time of 1 and 6 h post dose. Skin biopsy punctures were weighed directly following collection. Each skin puncture count was measured using a gamma counter (Wallac Wizard 1480, Perkin Elmer, Waltham, MA) and percent bound to the SC tissue was calculated. The 1-h post dose timepoint skin punctures radioactive count for each mAb was considered 100% bound for data normalization purposes. The 6-h post dose collected radioactivity data were compared reported as a fraction of the percent bound relative to the 1-h post dose timepoint for calculation, data processing and loss of mAb from the SC site reporting over time.

Abbreviations

SC	subcutaneous
mAb	monoclonal antibody
ECM	extracellular matrix
GAGs	glycosaminoglycans
PBS	phosphate-buffered saline
cIEF	capillary isoelectric focusing
DSC	differential scanning calorimetry
T_m	Temperature of melting
C_p	specific heat
$T_{m\ onset}$	onset of tertiary structure unfolding
T_{agg}	onset of aggregation
CM	center of mass
SLS	static light scattering
HIC	hydrophobic interaction chromatography
NaCl	sodium chloride
HP	heparin binding
T_i	elution time
T_0	column equilibrium time
T_e	end of gradient time
AUP	animal use protocol
IACUC	institutional animal care and use committee
TMB	3, 3', 5, 5'-tetramethylbenzidine
LLOQ	lower limit of quantitation
C_{max}	maximal concentration
CL	absolute clearance
CL/F	apparent clearance
%F	percent bioavailability
T_{max}	time at maximal concentration
IgGs	immunoglobulins
CDR	complementarity-determining region
FcRn	neonatal Fc receptor
k_a	rate of absorption
K_D	equilibrium dissociation constant
kDa	kilodalton
SD	standard deviation
^{125}I	Iodine 125
AUC	area under the curve
IV	intravenous
pI	isoelectric point
PK	pharmacokinetics
PK/PD	pharmacokinetics and pharmacodynamic
TMDD	target-mediated drug disposition
HIP	hydrophobic interaction potential
HpnIP	heparin interaction potential.

Disclosure of Potential Conflicts of Interest

No potential conflicts of interest were disclosed.

ORCID

Amita Datta-Mannan  <http://orcid.org/0000-0003-2365-5360>

References

- Kaplon H, Reichert JM. Antibodies to watch in 2018. *mAbs*. 2018;10:183–203.
- Kaplon H, Muralidharan M, Schneider Z, Reichert JM. Antibodies to watch in 2020. *mAbs*. 2020;12:1703531. doi:10.1080/19420862.2019.1703531.
- Matucci A, Vultaggio A, Danesi R. The use of intravenous versus subcutaneous monoclonal antibodies in the treatment of severe asthma: a review. *Respir Res*. 2018;19:154. doi:10.1186/s12931-018-0859-z.
- Viola M, Sequeira J, Seica R, Veiga F, Serra J, Santos AC, Ribeiro AJ. Subcutaneous delivery of monoclonal antibodies: how do we get there? *J Control Release*. 2018;286:301–14. doi:10.1016/j.jconrel.2018.08.001.
- Lobo ED, Hansen RJ, Balthasar JP. Antibody pharmacokinetics and pharmacodynamics. *J Pharm Sci*. 2004;93:2645–68. doi:10.1002/jps.20178.
- Turner MR, Balu-Iyer SV. Challenges and opportunities for the subcutaneous delivery of therapeutic proteins. *J Pharm Sci*. 2018;107:1247–60. doi:10.1016/j.xphs.2018.01.007.
- Wang W, Wang EQ, Balthasar JP. Monoclonal antibody pharmacokinetics and pharmacodynamics. *Clin Pharmacol Ther*. 2008;84:548–58. doi:10.1038/clpt.2008.170.
- Richter WF, Jacobsen B. Subcutaneous absorption of biotherapeutics: knowns and unknowns. *Drug Metab Dispos*. 2014;42:1881–89. doi:10.1124/dmd.114.059238.
- Charman SA, McLennan DN, Edwards GA, Porter CJ. Lymphatic absorption is a significant contributor to the subcutaneous bioavailability of insulin in a sheep model. *Pharm Res*. 2001;18:1620–26. doi:10.1023/A:1013046918190.
- Dahlberg AM, Kaminskas LM, Smith A, Nicolazzo JA, Porter CJ, Bulitta JB. The lymphatic system plays a major role in the intravenous and subcutaneous pharmacokinetics of trastuzumab in rats. *Mol Pharm*. 2014;11:496–504. doi:10.1021/mp400464s.
- McLennan DN, Porter CJ, Edwards GA, Martin SW, Heatherington AC, Charman SA. Lymphatic absorption is the primary contributor to the systemic availability of epoetin Alfa following subcutaneous administration to sheep. *J Pharmacol Exp Ther*. 2005;313:345–51. doi:10.1124/jpet.104.078790.
- Datta-Mannan A, Witcher DR, Lu J, Wroblewski VJ. Influence of improved FcRn binding on the subcutaneous bioavailability of monoclonal antibodies in cynomolgus monkeys. *mAbs*. 2012;4(2):267–73. doi:10.4161/mabs.4.2.19364.
- Deng R, Loyet KM, Lien S, Iyer S, DeForge LE, Theil F-P, Lowman HB, Fielder PJ, Prabhu S. Pharmacokinetics of humanized monoclonal anti-tumor necrosis factor- α antibody and its neonatal Fc receptor variants in mice and cynomolgus monkeys. *Drug Metab Dispos*. 2010;38(4):600–05. doi:10.1124/dmd.109.031310.
- Kagan L, Mager DE. Mechanisms of subcutaneous absorption of rituximab in rats. *Drug Metab Dispos*. 2013;41:248–55. doi:10.1124/dmd.112.048496.
- Khawli LA, Goswami S, Hutchinson R, Kwong ZW, Yang J, Wang X, Yao Z, Sreedhara A, Cano T, Tesar DB. Charge variants in IgG1: isolation, characterization, in vitro binding properties and pharmacokinetics in rats. *mAbs*. 2010;2(6):613–24. doi:10.4161/mabs.2.6.13333.
- Zheng Y, Tesar DB, Benincosa L, Birnbock H, Boswell CA, Bumbaca D, Cowan KJ, Danilenko DM, Daugherty AL, Fielder PJ. Minipig as a potential translatable model for

- monoclonal antibody pharmacokinetics after intravenous and subcutaneous administration. *mAbs*. 2012;4(2):243–55. doi:10.4161/mabs.4.2.19387.
17. Mach H, Gregory SM, Mackiewicz A, Mittal S, Lalloo A, Kirchmeier M, Shameem M. Electrostatic interactions of monoclonal antibodies with subcutaneous tissue. *Ther Deliv*. 2011;2(6):727–36. doi:10.4155/tde.11.31.
 18. Datta-Mannan A, Lu J, Witcher DR, Leung D, Tang Y, Wroblewski VJ. The interplay of non-specific binding, target-mediated clearance and FcRn interactions on the pharmacokinetics of humanized antibodies. *mAbs*. 2015;7:1084–93. doi:10.1080/19420862.2015.1075109.
 19. Datta-Mannan A, Thangaraju A, Leung D, Tang Y, Witcher DR, Lu J, Wroblewski VJ. Balancing charge in the complementarity-determining regions of humanized mAbs without affecting pI reduces non-specific binding and improves the pharmacokinetics. *mAbs*. 2015;7(3):483–93. doi:10.1080/19420862.2015.1016696.
 20. Datta-Mannan A, Chow CK, Dickinson C, Driver D, Lu J, Witcher DR, Wroblewski VJ. FcRn affinity-pharmacokinetic relationship of five human IgG4 antibodies engineered for improved in vitro FcRn binding properties in cynomolgus monkeys. *Drug Metab Dispos*. 2012;40:1545–55. doi:10.1124/dmd.112.045864.
 21. Chaparro-Riggers J, Liang H, DeVay RM, Bai L, Sutton JE, Chen W, Geng T, Lindquist K, Casas MG, Boustany LM. Increasing serum half-life and extending cholesterol lowering in vivo by engineering antibody with pH-sensitive binding to PCSK9. *J Biol Chem*. 2012;287(14):11090–97. doi:10.1074/jbc.M111.319764.
 22. Datta-Mannan A, Wroblewski VJ. Application of FcRn binding assays to guide mab development. *Drug Metab Dispos*. 2014;42:1867–72. doi:10.1124/dmd.114.059089.
 23. Igawa T, Ishii S, Tachibana T, Maeda A, Higuchi Y, Shimaoka S, Moriyama C, Watanabe T, Takubo R, Doi Y. Antibody recycling by engineered pH-dependent antigen binding improves the duration of antigen neutralization. *Nat Biotechnol*. 2010;28(11):1203–07. doi:10.1038/nbt.1691.
 24. Yeung YA, Wu X, Reyes AE 2nd, Vernes JM, Lien S, Lowe J, Maia M, Forrest WF, Meng YG, Damico LA. A therapeutic anti-VEGF antibody with increased potency independent of pharmacokinetic half-life. *Cancer Res*. 2018;10(8):3269–77. doi:10.1158/0008-5472.CAN-09-4580.
 25. Igawa T, Tsunoda H, Tachibana T, Maeda A, Mimoto F, Moriyama C, Nanami M, Sekimori Y, Nabuchi Y, Aso Y. Reduced elimination of IgG antibodies by engineering the variable region. *Protein Eng Des Sel*. 2010;23(5):385–92. doi:10.1093/protein/gzq009.
 26. Li B, Tesar D, Boswell CA, Cahaya HS, Wong A, Zhang J, Meng YG, Eigenbrot C, Pantua H, Diao J. Framework selection can influence pharmacokinetics of a humanized therapeutic antibody through differences in molecule charge. *mAbs*. 2014;6(5):1255–64. doi:10.4161/mabs.29809.
 27. Sampei Z, Igawa T, Soeda T, Okuyama-Nishida Y, Moriyama C, Wakabayashi T, Tanaka E, Muto A, Kojima T, Kitazawa T. Identification and multidimensional optimization of an asymmetric bispecific IgG antibody mimicking the function of factor VIII cofactor activity. *PLoS One*. 2013;8(2):e57479. doi:10.1371/journal.pone.0057479.
 28. Datta-Mannan A, Witcher DR, Tang Y, Watkins J, Jiang W, Wroblewski VJ. Humanized IgG1 variants with differential binding properties to the neonatal Fc receptor: relationship to pharmacokinetics in mice and primates. *Drug Metab Dispos*. 2007;35:86–94. doi:10.1124/dmd.106.011734.
 29. Datta-Mannan A, Witcher DR, Tang Y, Watkins J, Wroblewski VJ. Monoclonal antibody clearance. Impact of modulating the interaction of IgG with the neonatal Fc receptor. *J Biol Chem*. 2007;282:1709–17.